Front. Chem. Sci. Eng. 2023, 17(1): 102−115
https://doi.org/10.1007/s11705-022-2179-6

RESEARCH ARTICLE

Synergistic effect of V and Fe in Ni/Fe/V ternary layered double hydroxides for efficient and durable oxygen evolution reaction

Lihong Chen[1], Ruxin Deng[1], Shaoshi Guo[1], Zihuan Yu[1], Huiqin Yao (✉)[2], Zhenglong Wu (✉)[3], Keren Shi[4], Huifeng Li (✉)[1], Shulan Ma (✉)[1]

1 Beijing Key Laboratory of Energy Conversion and Storage Materials, College of Chemistry, Beijing Normal University, Beijing 100875, China
2 School of Basic Medical Sciences, Ningxia Medical University, Yinchuan 750004, China
3 Analytical and Testing Center, Beijing Normal University, Beijing 100875, China
4 State Key Laboratory of High-efficiency Utilization of Coal and Green Chemical Engineering, Ningxia University, Yinchuan 750021, China

Abstract High-performance and stable electrocatalysts are vital for the oxygen evolution reaction (OER). Herein, via a one-pot hydrothermal method, Ni/Fe/V ternary layered double hydroxides (NiFeV-LDH) derived from Ni foam are fabricated to work as highly active and durable electrocatalysts for OER. By changing the feeding ratio of Fe and V salts, the prepared ternary hydroxides were optimized. At an Fe:V ratio of 0.5:0.5, NiFeV-LDH exhibits outstanding OER activity superior to that of the binary hydroxides, requiring overpotentials of 269 and 274 mV at 50 mA·cm^{-2} in the linear sweep voltammetry and sampled current voltammetry measurements, respectively. Importantly, NiFeV-LDH shows extraordinary long-term stability (⩾ 75 h) at an extremely high current density of 200 mA·cm^{-2}. In contrast, the binary hydroxides present quick decay at 200 mA·cm^{-2} or even reduced current densities (150 and 100 mA·cm^{-2}). The outstanding OER performance of NiFeV-LDH benefits from the synergistic effect of V and Fe while doping the third metal into bimetallic hydroxide layers: (a) Fe plays a crucial role as the active site; (b) electron-withdrawing V stabilizes the high valence state of Fe, thus accelerating the OER process; (c) V further offers great stabilization for the formed intermediate of FeOOH, thus achieving superior durability.

Keywords oxygen evolution reaction, electrocatalysts, ternary layered double hydroxides, long-term stability

1 Introduction

With the increasing power demand of human society and the rapid consumption of fossil fuels, the exploration of renewable energy has become a hot topic. Hydrogen, due to its high energy density and zero carbon emission, has been considered as a promising substitute [1]. Electrocatalytic water splitting can produce pure hydrogen, which involves two half-reactions, i.e., hydrogen evolution reaction (HER) and oxygen evolution reaction (OER) [2]. Compared to the relatively simple HER (a two electron-transfer reaction), the OER (a four electron-proton coupled reaction) requires an excessively high overpotential, which severely hinders water splitting [3]. Ru- and Ir-based materials are recognized as optimized electrocatalysts that can effectively reduce overpotentials [4]. However, due to their high cost and scarcity, their large-scale industrial application is hampered. For the design of electrocatalysts, high activity and economic applicability are important targets.

Recently, transition metal-based compounds have attracted considerable attention as non-noble OER catalysts. Layered double hydroxides (LDHs) are widely used two-dimensional materials composed of positively charged brucite host layers and interlayer anions to balance the charge. LDHs have many advantages such as high specific surface area, enriched chemically active sites, tunable laminate composition, exchangeable guest anions and low-cost manufacturing processes [5]. Recently, transition-metal-based LDHs have been reported to exhibit outstanding electrocatalytic activity toward OER, especially Ni-based LDHs [6–8]. In comparison with bimetallic LDHs, ternary LDHs usually

Received February 14, 2022; accepted April 29, 2022

E-mails: huiqin_yao@163.com (Yao H.), wuzl@bnu.edu.cn (Wu Z.), lihuifeng@bnu.edu.cn (Li H.), mashulan@bnu.edu.cn (Ma S.)

display improved electrocatalytic performance [9], which benefits from the optimized electron structure due to the synergistic effect among the metal ions. Bi et al. [10] reported that incorporation of cobalt into NiFe-LDH caused a smaller onset potential, and the introduced Co ions in varied valence depicted different effects on OER; for instance, Co^{2+} helped to reduce the overpotential of the formed intermediate active substance of *OOH, while the doping of Co^{3+} accelerated the deprotonation step during OER. Via a coprecipitation method by adding NaOH into an aqueous solution of $NiCl_2$, VCl_3 and $FeCl_3$, Fe-doped NiV-LDH was fabricated [11], showing enhanced OER activity with an overpotential of 269 mV at 10 mA·cm^{-2} (η_{10} = 269 mV). The good OER performance can be attributed to Fe^{3+} doping, which increased the oxidation capacity of Ni^{3+} and improved the charge transport of NiV-LDH. The phenomenon that Fe incorporation increases OER activity in catalysts is called the 'Fe effect' [12]. The dominance of Fe^{3+} ions in enhancing OER performance over other 3d trivalent cations (such as Co^{3+}, Mn^{3+}, Cr^{3+}, and V^{3+}) has been well-verified and greatly emphasized [13].

In addition to activity, stability is another important criterion to assess an electrocatalyst. In particular, long-term stability at high current density guarantees the industrialization of electrocatalysts. The V-based catalysts have been found to exhibit superior OER stability. For example, FeOOH-containing $Fe_5V_{15}O_{39}(OH)_9 \cdot 9H_2O$ can steadily operate for 36 h at 100 mA·cm^{-2} [14], and NiV-LDH@FeOOH may remain at a 95% current density within a 20 h test at 100 mA·cm^{-2} [15]. The synergistic effect of Fe and V has been explored, and it is found that V can offer considerable stabilization for unstable FeOOH [16]. Actually, the oxyhydroxide of FeOOH generated from surface reconstruction during OER was considered the real active species [17]. Thus, it is possible to simultaneously realize superior catalytic activity and high stability by integrating Fe and V into one electrocatalyst.

Besides, from the perspective of catalyst application, integrating active materials with conductive and robust substrates to fabricate self-supported electrodes can both improve the electrical conductivity and enhance mechanical strength. Ni foam, which has an interlinked cellular structure with high porosity > 95% and extremely large surface area, is widely utilized to overcome the barrier of low electron transfer efficiency. Meanwhile, Ni foam can offer a growth scaffold for other species. Additionally, Ni foam can act as a Ni source to produce Ni-based materials. Through a hydrothermal method using Ni foam as a Ni source, Yu et al. [18] prepared an efficient and stable NiFe-LDH catalyst (η_{10} = 211 mV), which can be steadily operated at 100 mA·cm^{-2} for 60000 s. Analogously, without adding any metal salts, Zeng et al. [19] gave Fe–Ni bimetallic foam a hydrothermal treatment in a KOH aqueous solution to obtain an Fe–Ni hydroxide nanosheet network (η_{10} = 261 mV), retaining a current density of 10 mA·cm^{-2} for 14 h without clear attenuation. Li et al. [20] prepared V-doped NiFe-LDH as an OER catalyst (η_{20} = 195 mV, remaining 98% of the current density of 187 mA·cm^{-2} after 18 h), while in the synthesis, $Ni(NO_3)_2$ was added as the Ni source. However, the preparation is material-consuming compared with approaches that do not use adscititious Ni.

Herein, through a one-step hydrothermal reaction using Ni foam as the substance and Ni source, we design a ternary LDH of Ni/Fe/V. The molar ratios of Fe and V were adjusted to optimize the OER property. At an Fe:V molar ratio of 0.5:0.5, the as-prepared NiFeV-LDH requires overpotentials of 269 and 274 mV at 50 mA·cm^{-2} (without iR drop compensation) in linear sweep voltammetry (LSV) and sampled current voltammetry (SCV) measurements, respectively. More importantly, NiFeV-LDH exhibits excellent long-term durability ($\geqslant$ 75 h) at a very high current density of 200 mA·cm^{-2}, providing an important guarantee for large-scale hydrogen production. The synergistic effect of Fe and V contributes to the superior OER catalytic activity and stability of ternary NiFeV-LDH compared to the two conventional LDH materials. This work provides new insights for the design of metal foam-derived self-supporting ternary LDH electrode materials applied for efficient and durable OER.

2 Experimental

2.1 Preparation of LDH-based electrocatalysts

A series of NiFeV-LDH materials were prepared via a facile one-step hydrothermal method. Different Fe:V molar ratios (Fe:V = 0:1, 0.3:0.7, 0.5:0.5, 0.7:0.3 and 1:0) were used, while the total amount of Fe + V was fixed at 2 mmol. Taking the sample with an Fe:V ratio of 0.5:0.5 as an example, 1 mmol (0.157 g) VCl_3, 1 mmol (0.404 g) $Fe(NO_3)_3 \cdot 9H_2O$, and 10 mmol (0.61 g) urea were dissolved in 35 mL of distilled water and stirred to obtain a homogenous solution. The mixed solution was transferred into a 50-mL Teflon-lined autoclave. Two pieces of pretreated Ni foam (4 cm× 1 cm) were added to the solution and reacted at 120 °C for 12 h. After the autoclave was cooled to room temperature, the as-synthesized NiFeV-LDH was collected and subsequently rinsed with distilled water and ethanol and dried in a vacuum oven at 60 °C overnight. The average mass loading of NiFeV-LDH on Ni foam was approximately 1.5 mg·cm^{-2}. The products synthesized at molar ratios of Fe:V of 0:1 (no Fe) and 1:0 (no V) are defined as NiV-LDH and NiFe-LDH, respectively.

2.2 Electrochemical measurements

Electrochemical measurements were performed on a

CHI660E electrochemical workstation with a three-electrode system at room temperature. An Hg/HgO electrode and graphite rod were used as the reference and counter electrodes, respectively. The as-prepared LDH derived from Ni foam with a size of 1 cm × 1 cm was used as a self-supported working electrode. An O_2-saturated 1 mol·L^{-1} KOH aqueous solution was used as the electrolyte. All potentials from electrochemical measurements were converted to reversible hydrogen electrode (RHE) using the following equation: $E_{RHE} = E_{Hg/HgO} + 0.059 \times pH + 0.098$ [21]. LSV were recorded with a sweep rate of 5 mV·s^{-1} and without *iR* drop compensation. The overpotential (η) was calculated using the equation: $\eta = E_{RHE} - 1.23$ V. A steady-state technique (here, SCV) was utilized to avoid potentially detrimental exaggeration of activity by LSV. Via sampling the OER current density at the 150th second of chronoamperometry (CA) responses acquired at 1.25, 1.30, 1.35, 1.40, 1.45, 1.50, 1.55, 1.60, 1.65, 1.70, 1.75, and 1.80 V (an interval of 0.05 V) for 180 s, the steady-state polarization curves were constructed, and corrected for an *iR* drop (by 40%) taking the uncompensated resistance (R_u) from electrochemical impedance spectroscopy (EIS) measurements, using the equation of $\eta = E_{RHE} - 1.23V - 40\% \cdot i \cdot R_u$ (*i* refers to the current). Tafel plots were derived from the 40% *iR* corrected steady-state polarization curves based on the Tafel equation [22]: $\eta = b \log j + a$ (*a* is a constant, *b* refers to the Tafel slope). The EIS measurements were performed at constant potentials (1.45, 1.50, 1.55, 1.60, 1.65, 1.70, 1.75 V vs. RHE). The frequency range is from 0.1 Hz to 100 kHz, and the AC amplitude is 5 mV. The cyclic voltammetry (CV) method was used to determine the absolute electrochemical active surface area (ECSA) values with a scan rate of 5 mV·s^{-1} in the region of 1.20–1.60 V vs. RHE. The CV curves were recorded at different scan rates (2, 4, 6, 8, 10 mV·s^{-1}) in the range of 1.2–1.3 V (vs. RHE), and the electrochemical double layer capacitance (Cdl) was estimated by determining the slope from a linear relationship between j (= $j_a - j_c$, j_a and j_c refer to the anodic and cathodic current densities at 1.25 V vs. RHE, respectively) and the scan rate. Chronopotentiometry curves were obtained from *I–t* tests implemented at current densities of 100, 150 and 200 mA·cm^{-2} for NiFe-LDH, NiV-LDH and NiFeV-LDH, respectively. For comparison, RuO_2 (loaded on Ni foam with 1.50 mg·cm^{-2}) and bare Ni foam were employed for OER measurements.

3 Results and discussion

Figure 1 shows the synthesis process of NiFeV-LDH via a one-pot hydrothermal reaction. Ni foam served as both the support and Ni source. $Fe(NO_3)_3 \cdot 9H_2O$ and VCl_3 were taken as Fe and V sources while urea was used as a precipitant. The influence of Fe:V feeding ratio was studied. LDHs based on different molar ratios of Fe:V (0:1, 0.3:0.7, 0.5:0.5, 0.7:0.3 and 1:0) were synthesized under the fixed total amount of Fe + V (2 mmol). ICP results (Table S1, cf. Electronic Supplementary Material, ESM) demonstrate that the atomic ratio of Fe:V in the obtained products is close to the molar ratios of the starting materials.

Figure 2 shows the powder X-ray diffraction (XRD) patterns of the as-prepared LDH materials. For all samples, there are observed three strongest reflections at 44.5°, 51.8° and 76.4° (labeled as '#') assigned to Ni^0 metals of the Ni substrate (JCPDF: 04-0850). For NiFeV-LDH (Fig. 2(a)), a series of diffraction peaks at 11.7°, 23.6°, 34.8°, 39.3°, 46.9°, 60.0° and 61.5° are assigned to the (003), (006), (012), (015), (018), (110) and (113) planes, suggesting a hexagonal crystal phase. The basal spacing (d_{basal}) of 0.758 nm is consistent with the reported CO_3^{2-} intercalated LDH with d_{basal} of 0.74–0.78 nm [23]. The d_{basal} values of NiFe-LDH (Fig. 2(b)) and NiV-LDH (Fig. 2(c)) are 0.769 and 0.752 nm, respectively.

The difference in the d_{basal} of the three types of LDHs is caused by the substitution effect of different ions in the lattice matrix [11]. According to Forano et al. [24], the difference in interlayer spacing can be attributed to the influence of metallic ions with different ionic radii. In LDH, when the bivalent ions (here, Ni^{2+}) are the same, the charge density of the layers depends on the radius of the trivalent ions, and the smaller is the ionic radius, the higher is the charge density of the layers. The local charge density of the layers affects the layer-anion interactions, i.e., the interlayer spacing [25,26]. Here, the

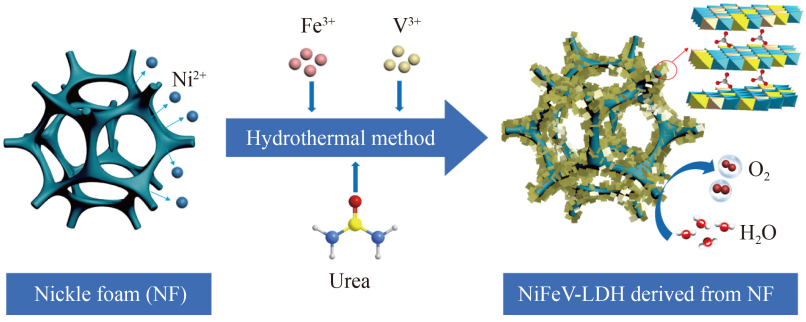

Fig. 1 Schematic illustration of the synthesis of NiFeV-LDH derived from Ni foam via a one-pot hydrothermal reaction.

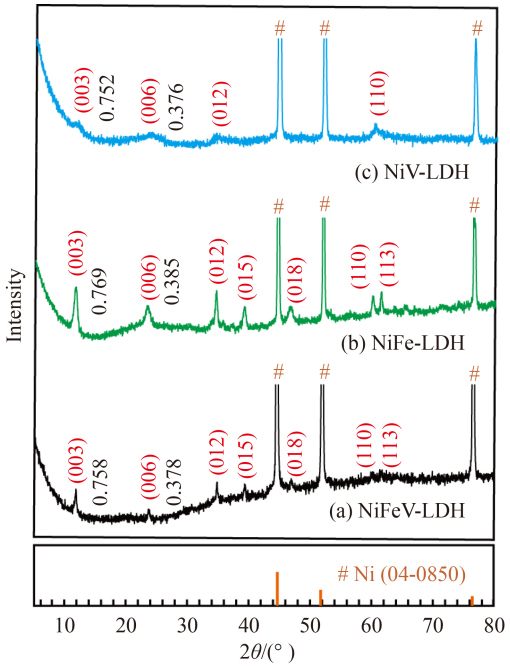

Fig. 2 XRD patterns of (a) NiFeV-LDH, (b) NiFe-LDH and (c) NiV-LDH (*d*-values in nm).

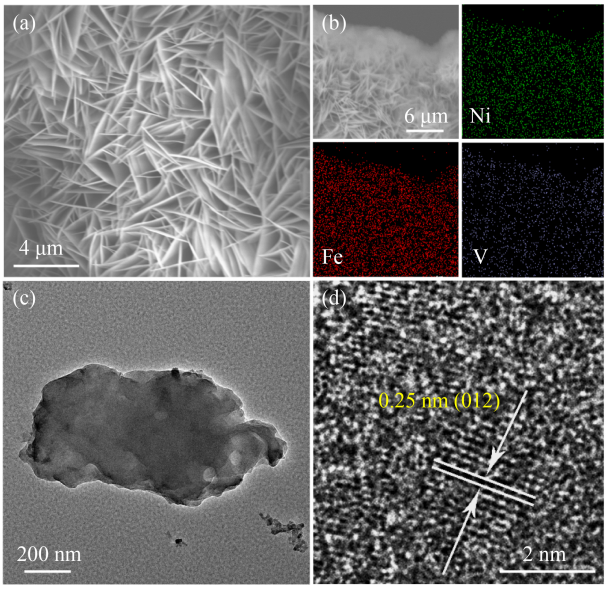

Fig. 3 (a) SEM image; (b) EDS elemental mapping (Ni, Fe and V); (c) TEM image; (d) HRTEM image of NiFeV-LDH.

ionic radius of Fe^{3+} of 0.645 Å is larger than that (0.640 Å) of V^{3+}. Additionally, V^{3+} can be easily oxidized to V^{4+} (0.580 Å) and V^{5+} (0.540 Å) with much smaller radii [27]. Thus, the charge density of NiFe-LDH layers would be lower than that of NiV-LDH layers, thus resulting in a larger interlayer spacing (0.769 nm). With the increased Fe content (decreased V content) (Fig. S1, cf. ESM), the d_{basal} values of the LDH samples increase, further confirming the abovementioned conclusions. The sharper and stronger diffraction peaks of NiFeV-LDH and NiFe-LDH indicate that the presence of Fe is beneficial to the improvement of the crystallization of the LDH materials. From another perspective, the introduction of V into NiFe-LDH decreases the crystallinity. This may be caused by the generation of a localized amorphous phase after doping. The crystallinity of hydroxides plays a critical role in catalytic activity. Song et al. [28] reported that doping-induced localized amorphization in α-$Ni(OH)_2$ could provide more accessible active sites than fully crystallized structures, thus boosting OER activity. In addition, performance enhancements in the electrocatalysis of water splitting utilizing amorphous materials as catalysts have been widely reported [29]. This inspires us that the controllable crystallinity of NiFeV-LDH achieved by adjusting the molar ratio of Fe and V may provide an opportunity for promoting its catalytic performance.

Scanning electron microscopy (SEM) and transmission electron microscopy (TEM) measurements were performed to characterize the morphology of the LDH materials, and the results are shown in Fig. 3. From Fig. 3(a), we observe that interconnected NiFeV-LDH nanosheet arrays uniformly vertically grow on Ni foam. These interlaced nanosheets with a lateral size of ~3 μm constitute a three dimensional (3D) porous firm network nanoarchitecture, which can expose as many active sites as possible and provide convenience for electrolyte transport and the release of the generated gas during water splitting. Energy dispersive spectroscopy (EDS) mapping (Fig. 3(b)) shows the coexistence of three metallic elements of Ni, Fe and V and their uniform distribution throughout the material. The TEM image of NiFeV-LDH scraped from the Ni substance under ultrasonication treatment (Fig. 3(c)) has a nanosheet-like morphology. From the high resolution TEM (HRTEM) image (Fig. 3(d)), well-resolved lattice fringes are observed, and a spacing of 0.25 nm is assigned to the (012) plane of the LDH structure [11].

Of note, although the three LDHs (NiV-LDH, NiFe-LDH and NiFeV-LDH) all present nanosheet-like morphologies, there are still slight differences in the morphology among them (Fig. S2, cf. ESM). The NiV-LDH nanosheets (Figs. S2(a) and S2(a′)) are smaller and stack to form nanoflowers. The lateral size of NiFe-LDH (Figs. S2(b) and S2(b′)) is similar to that of NiFeV-LDH (Figs. S2(c) and S2(c′)), while the latter is more uniform in arrangement on the surface of the Ni foam. Reasonable arrangement of active substances on the substrate is particularly important to develop a robust nanostructure with maximized surface area to boost the OER activity and durability of the catalyst.

X-ray photoelectron spectroscopy (XPS) measurements were performed to determine the composition and elemental oxidation state of the LDH materials (Fig. 4). All peak positions were corrected using the C 1s peak (284.8 eV). Figure 4(a) shows the XPS survey spectra of NiV-LDH, NiFe-LDH and NiFeV-LDH, demonstrating

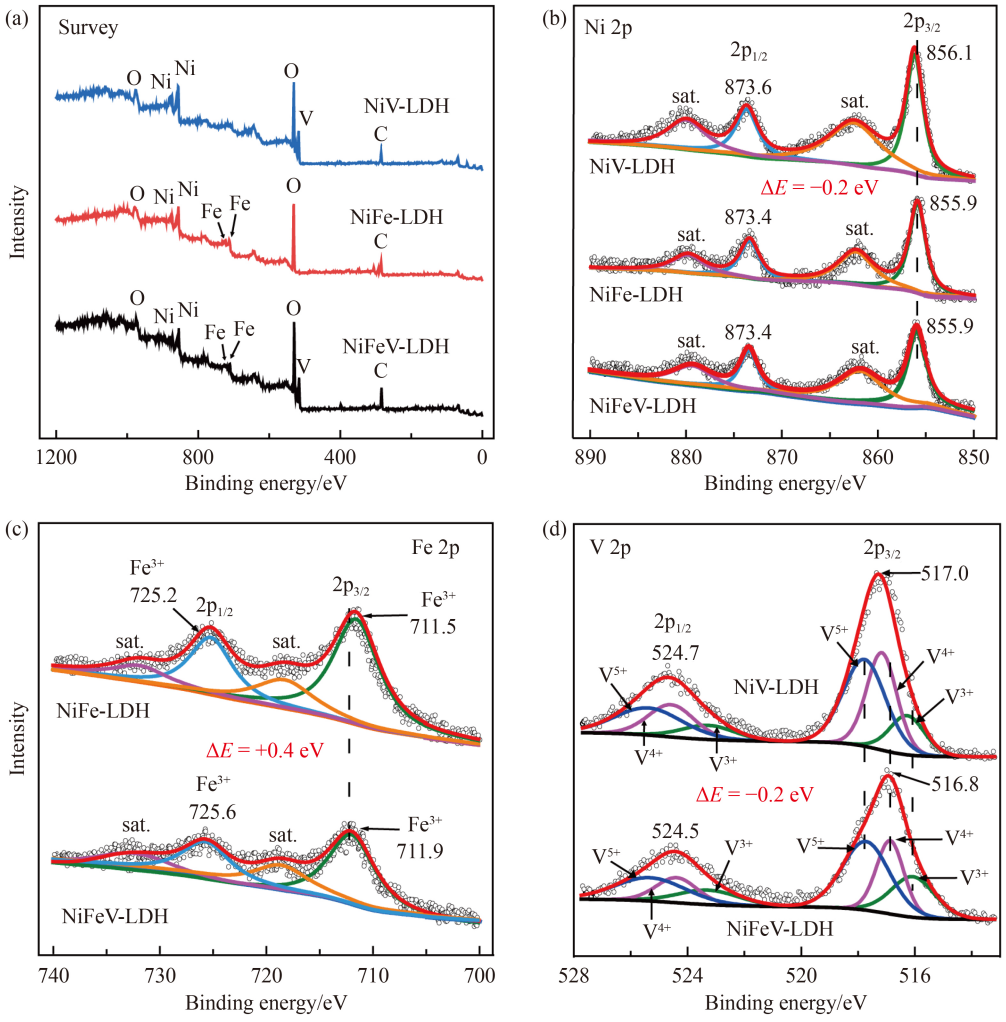

Fig. 4 (a) XPS survey and (b–d) XPS spectra with the deconvolution of corresponding XPS peaks: (b) Ni 2p of NiV-LDH, NiFe-LDH, and NiFeV-LDH, (c) Fe 2p of NiFe-LDH and NiFeV-LDH, (d) V 2p of NiV-LDH and NiFeV-LDH.

the presence of Ni, Fe, V and O in NiFeV-LDH, the absence of V in NiFe-LDH and the absence of Fe in NiV-LDH. From the Ni 2p spectra shown in Fig. 4(b), we see that NiFeV-LDH (with V) and NiFe-LDH (without V) have the same binding energies of 873.4 and 855.9 eV, corresponding to Ni $2p_{1/2}$ and Ni $2p_{3/2}$ of Ni^{2+} [30]. For NiFeV-LDH (having Fe), the binding energies (873.4 and 855.9 eV) of Ni^{2+} are lower than the energies (873.6 and 856.1 eV) of NiV-LDH (no Fe). Thus, in NiFeV-LDH, the valance state of Ni is mainly affected by Fe instead of by V, which is consistent with previous work reporting that V doping tends to modify the coordinating environment of Fe rather than Ni [20,31]. From the Fe 2p spectra shown in Fig. 4(c), NiFeV-LDH has two peaks at 725.6 and 711.9 eV assigned to Fe $2p_{1/2}$ and Fe $2p_{3/2}$ of Fe^{3+} [32]. Compared to the Fe(III) 2p energies (725.2 and 711.5 eV) of NiFe-LDH (without V), the Fe 2p peaks of NiFeV-LDH (with V) apparently shifted (+0.4 eV) to higher energies. This suggests that the presence of V leads to an increase in the valence state of Fe. Figure 4(d) shows the V 2p spectra. NiV-LDH exhibits peaks with binding energies of 524.7 and 517.0 eV attributed to V $2p_{1/2}$ and V $2p_{3/2}$, respectively. In contrast, NiFeV-LDH has lower binding energies of 524.5 (V $2p_{1/2}$) and 516.8 eV (V $2p_{3/2}$), giving a negative shift of 0.2 eV (–0.2 eV). The peak at 517.0 eV can be fitted into three peaks at 516.1, 517.0 and 517.6 eV, attributed to V^{3+}, V^{4+} and V^{5+}, and the peak at 516.8 eV can be fitted into three peaks at 515.9, 516.8 and 517.6 eV, attributed to V^{3+}, V^{4+} and V^{5+}, respectively [8,33]. The peak positions of V^{3+} and V^{4+} both show a negative shift after Fe doping, while that of V^{5+} remains unchanged. Based on the peak area integration information shown in Table S2 (cf. ESM), we see that the molar ratio of V^{3+}:V^{4+}:V^{5+} in NiV-LDH is 0.139:0.417:0.444. After Fe doping, the molar ratio of V^{3+}:V^{4+}:V^{5+} in NiFeV-LDH changes to 0.247:0.295:0.458. This result confirms that the electronic structure of NiV-LDH is modified after Fe introduction. The drastic reduction of V^{4+} and increase in V^{3+} along with the few changes in V^{5+} give us some inspiration for the deduction that V^{4+} may play a key role as an electron acceptor in the Fe doping process, and consequently, the percentage of V

ions with a lower oxidation state would rise. Certainly, the fact that V ions can be easily oxidized to high valance states in synthetic processes should not be ignored.

The change in binding energy implies that the chemical environment of related atoms has been changed. Based on the abovementioned discussions, we conclude that the electronic structures of the binary LDHs (NiFe-LDH or NiV-LDH) are tuned after the third metal ion (V or Fe) incorporation. Heteroatom doping of non-noble metal-based catalysts has been recognized as an effective electronic structure tuning strategy generally accompanied by improved conductivity, favorable adsorption ability and reduced kinetic energy barrier, thus boosting the catalytic performance [34]. In the ternary hydroxide NiFeV-LDH, the V tends to act as an electron acceptor, while Fe works as an electron donator, causing a negative shift of V (compared to NiV-LDH) and a positive shift of Fe (compared to NiFe-LDH). These results indicate the electron transfer from Fe to V. It has been reported that metals with higher oxidation states, such as Fe^{4+}, Ni^{4+}, W^{6+}, and Cr^{4+}, demonstrate higher OER performance owing to the optimized bond strength between the catalyst and the water molecules/intermediate species [14,35]. Some researchers achieved the goal of keeping the active sites for the high valence state in the LDH structure by doping W^{6+} or Mo^{6+} into the laminate [36,37]. This occurs from the electron-withdrawing effect of such metal ions with a higher valance state. In addition, V^{4+} and V^{5+} ions were also reported to be efficient in increasing the valence of adjacent 3d transition metals to accelerate the water oxidation reaction [37,38]. Here, we attribute the electron transfer from Fe to V observed from the XPS spectrum to the electron-withdrawing effect of high-valent V ions, which can help stabilize the high valence state of adjacent Fe. Apparently, the synergistic interaction of the ternary metal system is crucial to the OER activity of the ternary LDH material, which was verified in a later electrochemical test.

The OER performance of the as-prepared catalysts was measured, and the obtained results are shown in Fig. 5. From the iR drop uncompensated LSV (Fig. 5(a)), NiFeV-LDH exhibits the best catalytic OER activity, requiring extremely low overpotentials of 269, 320 and 408 mV to deliver large current densities of 50, 100, and 200 mA·cm^{-2}, that is, η_{50} = 269 mV, η_{100} = 329 mV, and η_{200} = 408 mV. In contrast, much higher overpotentials, such as 296, 351, 416 and 469 mV for NiFe-LDH, NiV-LDH, RuO_2 and bare Ni foam, respectively, are required at a current density of 50 mA·cm^{-2}. Table S3 (cf. ESM) shows that NiFeV-LDH exhibits prominent ascendancy over many reported non-noble OER catalysts. For example, Co^{2+}- and Co^{3+}-doped NiFe-LDH loaded on carbon fiber both need > 300 mV to drive the current density of 50 mA·cm^{-2} (η_{50} > 300 mV) [10]; Fe–Ni bime tallic foam-derived hydroxide possessed a moderate catalytic activity with an η_{50} of 290 mV [19], and the Ni foam-supported CoFeV LDH synthesized via a solvothermal method exhibited an η_{50} of 290 mV [38]. An electrochemical activated NiFeV-LDH (A-NiFeV-LDH), which was prepared through a combined strategy of hydrothermal and in situ electrochemical activation, presented an η_{50} of 310 mV [39]. The influence of the Fe:V feeding ratio on the OER performance of LDHs was also explored. Figure S3 (cf. ESM) shows the LSV curves and the histogram of overpotentials at 50 mA·cm^{-2} (η_{50}) and 100 mA·cm^{-2} (η_{100}) of the five LDH samples with different Fe:V ratios. At Fe:V molar ratios of 0:1, 0.3:0.7: 0.5:0.5, 0.7:0.3, and 1:0, the LDH materials give η_{50} values of 351, 285, 269, 276, and 296 mV, respectively, showing a trend from large to small and then increasing. The OER activity trend of LDH samples follows the Fe:V molar ratio of 0.5:0.5 > 0.7:0.3 > 0.3:0.7 > 1:0 (no V) > 0:1 (no Fe). We can conclude that the OER activity of all ternary LDHs is better than that of any of the binary LDHs (NiFe-LDH or NiV-LDH). At an Fe:V molar ratio of 1:1, the Ni/Fe/V LDH exhibits the optimal OER activity.

Considering that the activity determined from LSV can be overestimated [40], we further employed a steady-state technique, SCV, to estimate our electrocatalysts. The CA responses were acquired at 1.25, 1.30, 1.35, 1.40, 1.45, 1.50, 1.55, 1.60, 1.65, 1.70, 1.75, and 1.80 V (a regular interval of 0.050 V) for 180 s. Figures 5(b) and S4 (cf. ESM) show the CA responses of NiFeV-LDH and NiFe-LDH, NiV-LDH, RuO_2 and Ni foam. It is clear that the LDH samples possess higher OER current densities than RuO_2 and bare Ni foam at the same given potential. Meanwhile, the quick decay of current density at the potential beyond 1.7 V is also observed, which indicates that such high given potential is not proper for the steady operation of catalysts. Figure 5(c) shows the plots of the sampled current densities (sampling the OER current densities at the 150th second) against potential without *iR* correction. The η_{50} values of NiFeV-LDH, NiFe-LDH, NiV-LDH, RuO_2 and Ni foam are 274, 301, 358, 428 and 549 mV, respectively. There is a non-negligible difference in OER overpotential obtained from the LSV and SCV. However, the OER activity of ternary NiFeV-LDH is still better than that of the binary LDH catalysts RuO_2 and Ni foam. The sampled steady-state OER current densities are corrected for *iR* drop (40%) using the R_u (obtained from the EIS measurements). From Fig. 5(d), the corrected overpotentials at 50 mA·cm^{-2} of NiFeV-LDH, NiFe-LDH, NiV-LDH, RuO_2 and Ni foam are 257, 277, 333, 401 and 511 mV, respectively. Because the *iR* drop compensation method (automatic or manual compensation) and the percentage of *iR* drop compensation have a great influence on the value of overpotential, we emphasize the significance of using the uncompensated overpotentials at the benchmark current densities to compare the OER activity of catalysts from different studies [41].

Of note, the OER process involves four electron

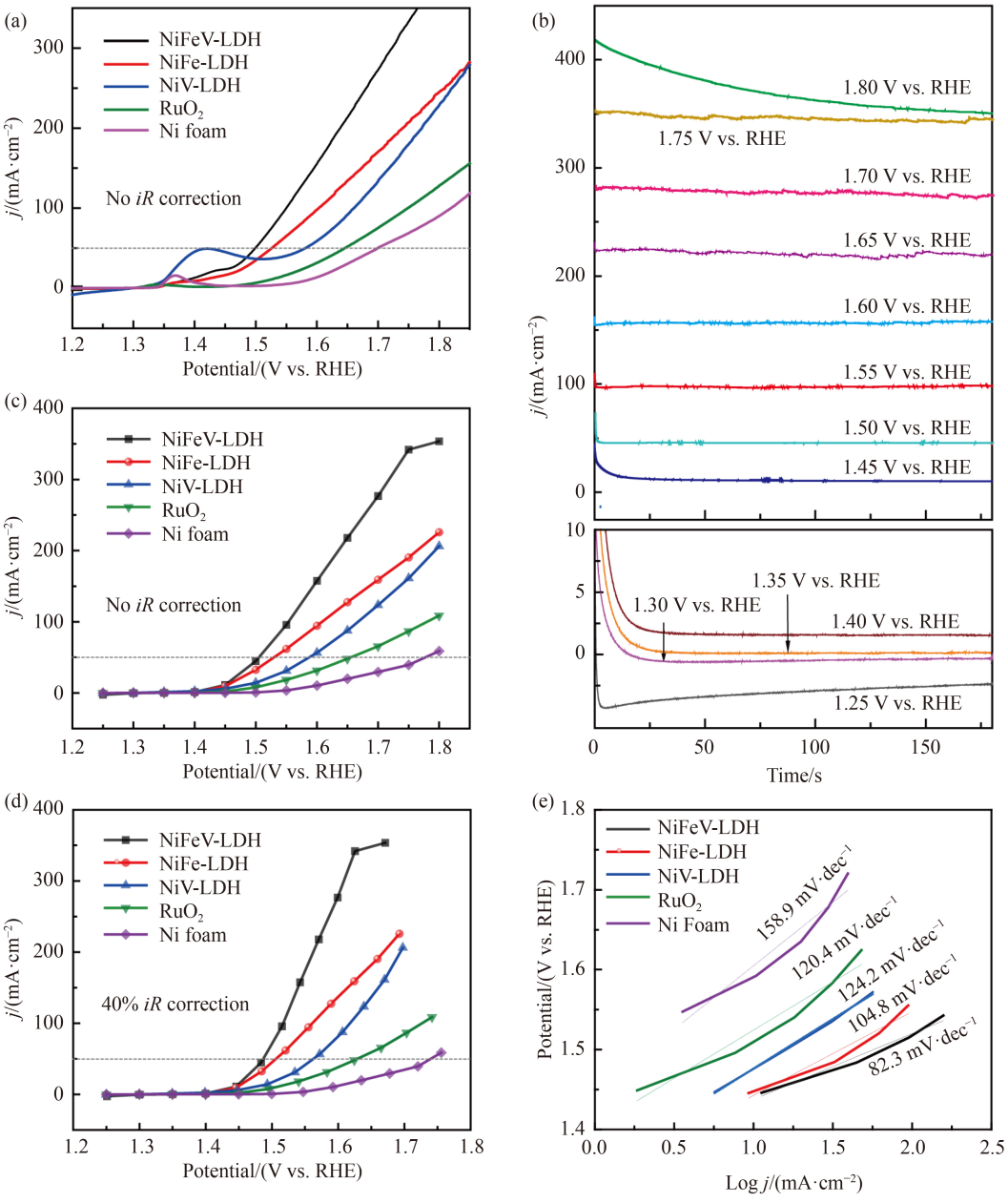

Fig. 5 (a) iR drop uncompensated OER LSV of NiFeV-LDH, NiFe-LDH, NiV-LDH, RuO_2 and Ni foam in 1.0 mol·L^{-1} KOH acquired with 5.0 mV·s^{-1}; (b) CA responses of NiFeV-LDH in 1.0 mol·L^{-1} KOH for 180 s, plots of sampled current densities against potential with (c) zero and (d) 40% *iR* drop compensation for NiFeV-LDH, NiV-LDH, RuO_2 and Ni foam, (e) the corresponding Tafel plots.

transfers, which are expressed by the following four equations: (1) $OH^- + * \rightarrow *OH + e^-$; (2) $*OH + OH^- \rightarrow *O + H_2O + e^-$; (3) $*O + OH^- \rightarrow *OOH + e^-$; (4) $*OOH + OH^- \rightarrow * + O_2 + H_2O + e^-$. Here, '*' denotes the catalyst active sites. The multiple electron transfer steps contribute to the sluggish kinetics of OER. Thus, OER electrocatalysts could accelerate the kinetics. To compare the OER kinetics of the catalysts, Tafel slopes can be calculated from the Tafel plots. The corresponding Tafel plots to steady-state polarization curves are shown in Fig. 5(e). The Tafel slopes of NiFeV-LDH, NiFe-LDH, NiV-LDH, RuO_2 and Ni foam are calculated to be 82.3, 104.8, 124.2, 120.4 and 158.9 mV·dec^{-1}, respectively. Generally, a smaller Tafel slope indicates that the current density can increase faster with a smaller overpotential change, implying faster electrocatalytic kinetics [42]. The NiFeV-LDH exhibits the lowest Tafel slope, suggesting that it has the fastest mass and electron transport rate. This may benefit from the synergistic effect among metal ions and the unique 3D porous structure of Ni foam with interconnected nanosheets growing vertically on it. In addition, the smaller Tafel slope of NiFe-LDH than that of NiV-LDH evidently promoted performance after Fe incorporation into binary LDH, confirming that Fe plays a

crucial role in the OER. Many theoretical and experimental studies have shown that Fe^{3+} sites have "fast" OER kinetics because they have optimum bond energetics for the adsorption of OER intermediates [12]. V, although it is not an active site for OER, makes important contributions to the improvement of kinetics by keeping high-valence state of active Fe^{3+} sites [20].

We adopted a well-known double layer capacitance method to determine the ECSA of the catalysts. Figure S5 shows the CV curves of NiFeV-LDH, NiFe-LDH and NiV-LDH at different scan rates (2, 4, 6, 8, 10 $mV \cdot s^{-1}$) and the corresponding Cdl values based on the potential at 1.25 V (vs. RHE). Notably, NiFeV-LDH possesses the largest Cdl of 26.1 $mF \cdot cm^{-2}$ compared to NiFe-LDH (22.7 $mF \cdot cm^{-2}$) and NiV-LDH (4.9 $mF \cdot cm^{-2}$). The larger ECSA of NiFeV-LDH allows more exposed active sites to promote OER performance. The vast difference in the Cdl value between Fe-containing LDH and NiV-LDH again confirms the great significance of Fe and suggests that Fe may act as the main active site. However, many reports have pointed out that not every ion adsorption site is a necessary OER active site [43]. Therefore, it is not entirely correct to compare the ECSA by calculating the Cdl values. For 3d-metal-based catalysts, we used the redox peak method [44] to calculate the surface concentration of the active sites (see the related calculation in the electronic supplementary material), and the obtained results are shown in Fig. 6.

Figure 6(a) shows the CV curves of NiFeV-LDH, NiFe-LDH, NiV-LDH, and Ni foam obtained from a backward sweep at 5 $mV \cdot s^{-1}$. Figure 6(b) shows that the integrated areas associated with the reduction of M(III) to M(II) for NiFeV-LDH, NiFe-LDH, NiV-LDH and Ni foam are 0.002465, 0.002043, 0.002008, and 0.0002417 VA, respectively. Hence, their associated charge values are 0.5290, 0.4086, 0.4017, and 0.04834 C. We obtained the absolute ECSA value by dividing the elementary charge of an electron, as shown in Fig. 6(c). The respective absolute ECSA values show that NiFeV-LDH benefits from the improved electrochemical surface area compared to the two binary LDH materials. It is clear that growing the active series on the bare Ni foam results in an exponential increase in the number of active sites. To distinguish the intrinsic OER activity differences of the LDH catalysts, we further report the specific activity by utilizing ECSA to normalize the current densities. To minimize the influence of the substrate (here, Ni foam), we revised the absolute ECSA value of NiFeV-LDH, NiFe-LDH, and NiV-LDH by subtracting that of the Ni foam. Then, we equated the ECSA of NiV-LDH to 1 and those of NiFeV-LDH and NiFe-LDH to 1.358 and 1.018, respectively [45]. Figure 6(d) shows the plots of the relative ECSA normalized sampled current densities against the *iR* corrected potential, and the turnover frequency (TOF) was also calculated and is shown in Fig. 6(e). The same trend of OER activity (NiFeV-LDH > NiFe-LDH > NiV-LDH) observed in Figs. 6(d) and 6(e) once again implies that our approach of doping the third metal into the binary LDH materials not only increases the ECSA but also enhances its intrinsic OER performance.

EIS was conducted to obtain more information about the electron transfer rate of the catalysts, and the results are shown in Fig. 7. To make a rational comparison, we performed the EIS measurements at constant potentials (1.45, 1.50, 1.55, 1.60, 1.65, 1.70, 1.75 V vs. RHE), and the resultant Nyquist and Bode absolute impedance plots are shown in Figs. 7(a–f) and S6 (cf. ESM). Given the small potential of 1.45 V vs. RHE, not every eletrocatalyst would undergo a charge-transfer controlled reaction, which is suggested by their Bode impedance plots and Nyquist plots. Figure 7(e) shows that NiV-LDH did not exhibit semicircle-shaped Nyquist plots until the potentials of the EIS measurements were increased to 1.60 V vs. RHE. It is not correct to compare the electron transfer rate of a set of catalysts at the potential that some of them do not begin water oxidation electrocatalysis but still exhibit capacitive behavior. Hence, we focused on the EIS plots obtained at potentials beyond 1.60 V vs. RHE. The radius of the semicircle of the Nyquist plot implies the value of the charge transfer resistance (R_{ct}). Clearly, at any potential beyond 1.60 V vs. RHE, the radius of the semicircle of the Nyquist plot (shown in Fig. 7(a)) for NiFeV-LDH is the smallest, implying that NiFeV-LDH has fast electron transport during the electrochemical reaction. Generally, a lower phase angle value in the Bode phase angle plot indicates a better charge transfer across the interface and a lower value. The ternary NiFeV-LDH has the smallest phase angle, which confirms that NiFeV-LDH is a superior active interface in the OER. As shown in Figs. 7(g) and 7(h), the fitting equivalent circuit model provides the specific R_{ct} values of the materials. R_{ct} decreases as the potential increases, which is consistent with a Faradaic process. The order of R_{ct} values of our five types of catalysts at 1.60, 1.65, 1.70, and 1.75 V vs. RHE is NiFeV-LDH < NiFe-LDH < NiV-LDH < RuO_2 < Ni foam. For example, the R_{ct} values of NiFeV-LDH, NiFe-LDH, NiV-LDH, RuO_2 and Ni foam at 1.75 V vs. RHE is 0.082, 0.16, 0.39, 0.98, and 2.51 Ω, respectively, which resonates well with the activity trend mentioned above. These results strongly confirm that NiFeV-LDH has a superfast electron transfer rate in the electrocatalytic process. This can be explained by the fact that Fe integration is effective in improving the electronic conductivity of Ni-based materials, consistent with previous reports [46]. The V incorporation further regulates the electronic structure of Fe, resulting in the most efficient electron conduction of NiFeV-LDH [20].

In addition to electrocatalytic activity, long-term stability at high current density is also an important characteristic of good electrocatalysts. The stability test results are shown in Fig. 8. Chronopotentiometry tests with current densities of 100, 150 and 200 $mA \cdot cm^{-2}$ for

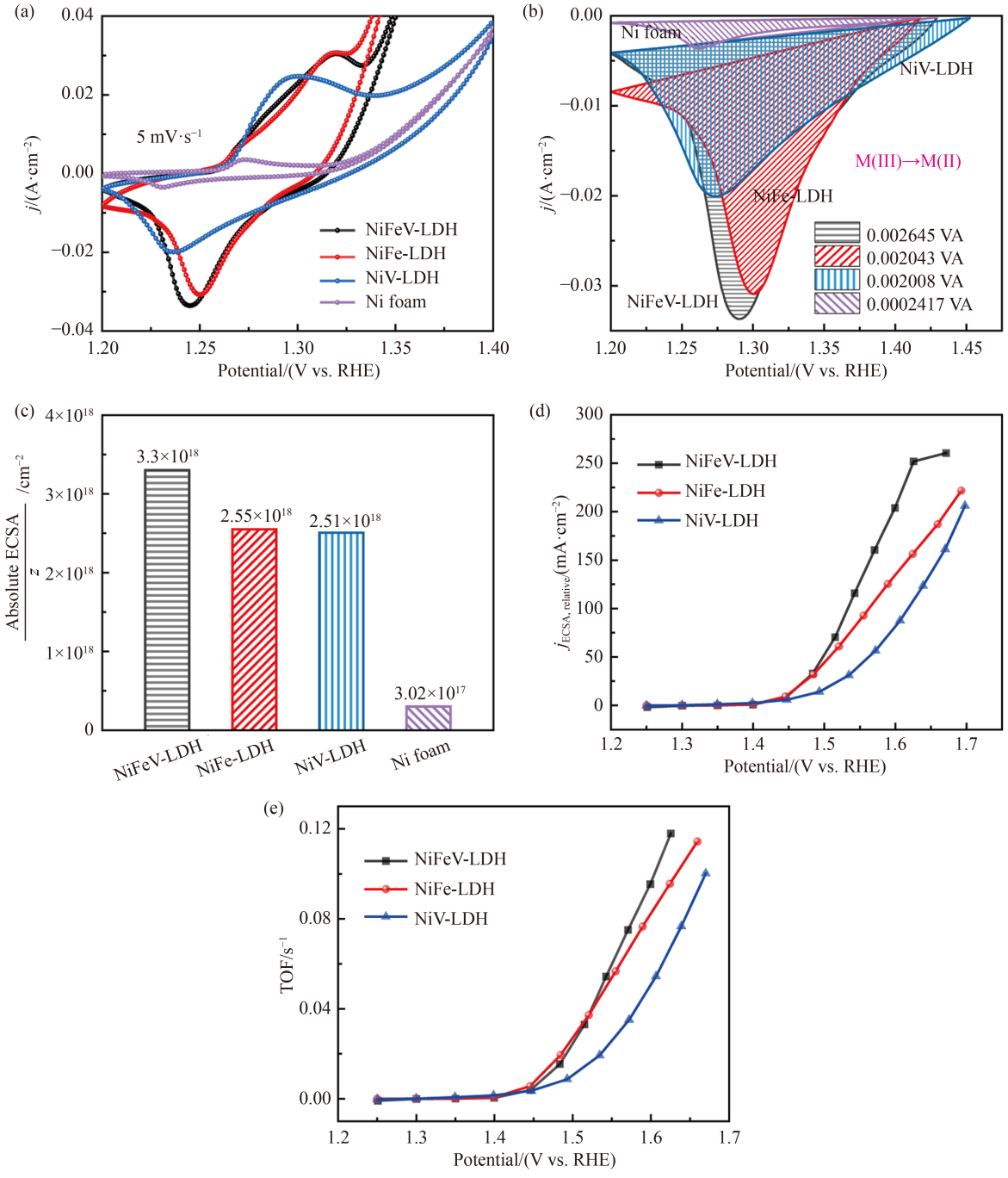

Fig. 6 (a) CV curves of NiFeV-LDH, NiFe-LDH, NiV-LDH and Ni foam; (b) the corresponding area of redox features considered for the calculation of the number of active sites; (c) absolute ECSA calculated by dividing the elementary charge of an electron for NiFeV-LDH, NiFe-LDH, NiV-LDH and Ni foam; (d) plots of the relative ECSA normalized sampled current densities against the *iR* corrected potential; (e) plots of TOF values as a function of potential.

NiFe-LDH, NiV-LDH and NiFeV-LDH were conducted. As shown in Fig. 8(a), at an extremely high current density of 200 mA·cm^{-2}, NiFeV-LDH shows superb stability with a 95% current density maintained after 75 h of OER testing. In contrast, NiFe-LDH and NiV-LDH present quick decay of the initial current density of 200 mA·cm^{-2}. At the lower current density of 150 mA·cm^{-2}, the NiV-LDH retains only 90% of the initial current density after 20 h of electrolysis, while NiFe-LDH shows quick decay at this current density. Therefore, we continued to study the stability at a much reduced current density of 100 mA·cm^{-2}, and NiFe-LDH only maintains 80% of the initial current density of 100 mA·cm^{-2} after electrolysis for 20 h. These results indicate that the V-containing LDHs possess increased electrocatalytic stability, and the synergy between V and Fe (electron transfer) is more conducive to the improvement of stability. Figure 8(b) shows the LSV curves recorded for

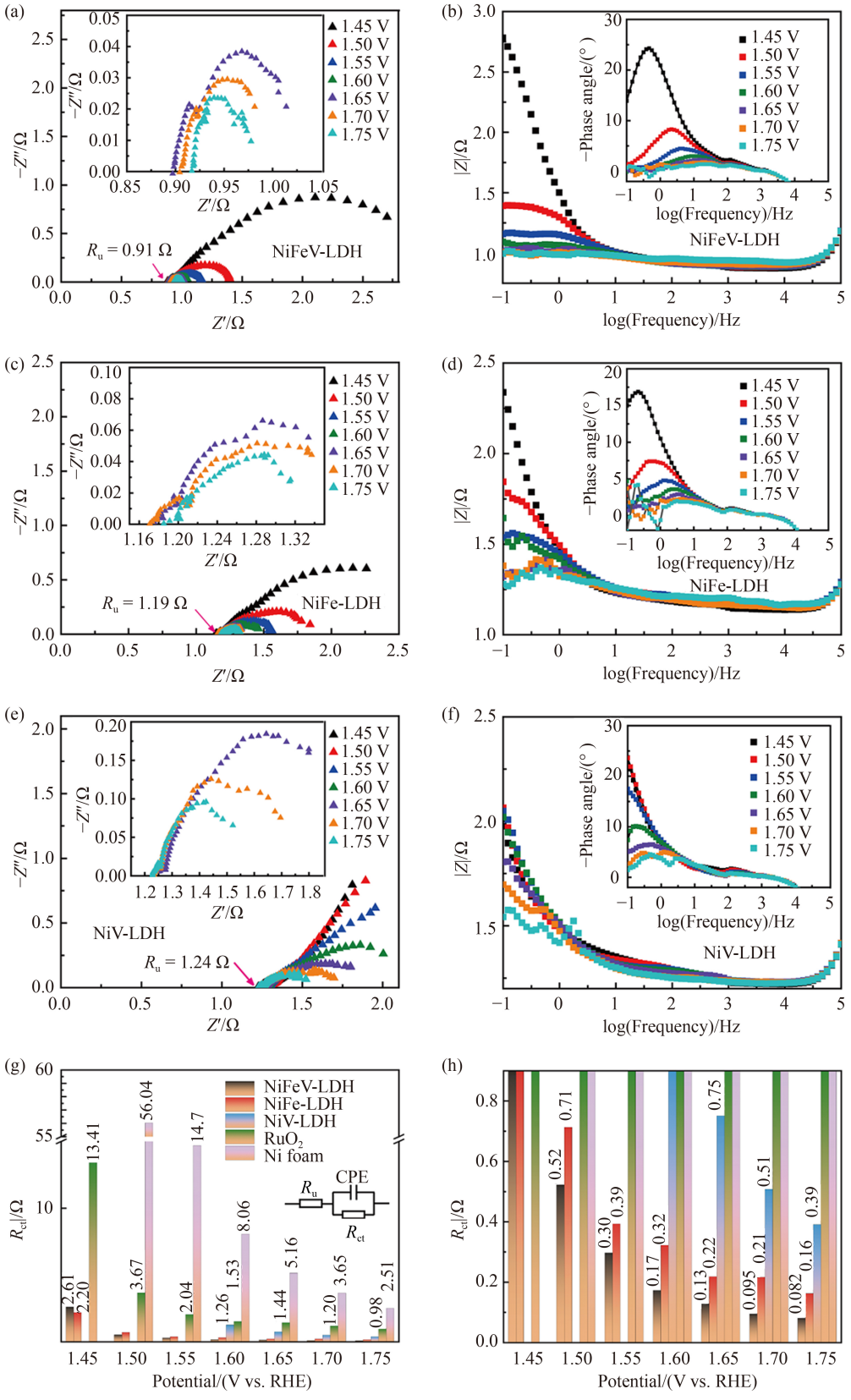

Fig. 7 Nyquist plots of (a) NiFeV-LDH, (c) NiFe-LDH, (e) NiV-LDH acquired at 1.45, 1.50, 1.55, 1.60, 1.65, 1.70, 1.75 V vs. RHE and (b, d, f) their corresponding Bode absolute impedance plots, (g, h) plots of R_{ct} values against 1.45, 1.50, 1.55, 1.60, 1.65, 1.70, 1.75 V vs. RHE for NiFeV-LDH, NiFe-LDH, NiV-LDH, RuO_2 and Ni foam.

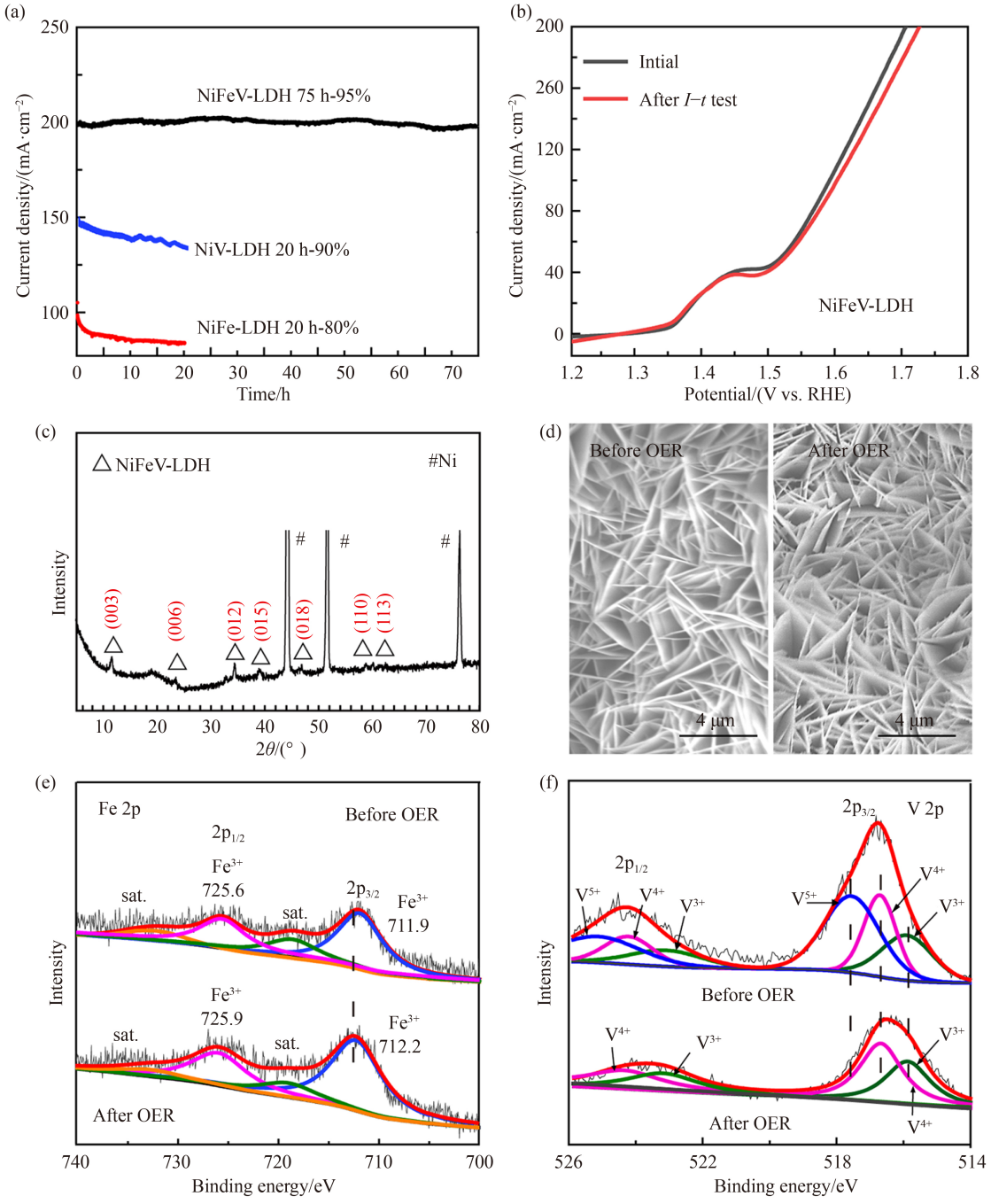

Fig. 8 (a) CA curves of NiFeV-LDH, NiFe-LDH and NiV-LDH; (b) LSV curves recorded for NiFeV-LDH before and after the *I–t* test (75 h); (c) XRD pattern of NiFeV-LDH after the OER durability test; (d) SEM images of NiFeV-LDH before and after the durability test; XPS spectra of (e) Fe 2p and (f) V 2p for NiFeV-LDH before and after the OER durability test.

NiFeV-LDH before and after the *I–t* test. As shown, there is a negligible degradation of current density, which indicates the good stability of NiFeV-LDH.

XRD, SEM and XPS analyses were performed to further explore whether there was structural change in NiFeV-LDH after the long-term stability test. As shown in Fig. 8(c), the XRD pattern of NiFeV-LDH after the *I–t* test is similar to that before the test. The SEM images shown in Fig. 8(d) indicate that NiFeV-LDH after the *I–t* test still retains the interlaced nanosheet-like morphology. XPS spectra of NiFeV-LDH after the *I–t* test shows that the Ni 2p spectra (Fig. S7, cf. ESM) remain the same as before. For Fe 2p shown in Fig. 8(e), the two new peaks at 712.2 and 725.9 eV indicate that Fe^{3+} can be partially oxidized into FeOOH during the OER [47]. For V 2p shown in Fig. 8(f), the existence of V^{3+} and V^{4+} in NiFeV-LDH after the *I–t* test exhibits the robust stability of the material. The disappearance of V^{5+} may be due to the release of the [VO_4] tetrahedron [39] arising from lattice distortion during the OER. Many articles have

reported that oxyhydroxides generated during surface reconstruction processes are the real active species for the OER. In other words, the materials we synthesized are only pre-catalysts and the real active centers only appear after the surface reconstruction processes [48]. For an OER catalyst employed in effective and practical electrocatalysis, a low activation energy barrier for initiating reconstruction and the stabilization of metastable active species are crucial but challenging to achieve. Luckily, we see that the ternary NiFeV-LDH possesses the lowest onset potential, which means that it has the fastest surface reconstruction kinetics among the examined catalysts. According to Fan's work [16], V^{3+} can easily dope into FeOOH and offer considerable chemical stabilization. In this way, we can explain well the large stability difference between NiFeV-LDH and NiFe-LDH. In the alkaline solution (1 mol·L^{-1} KOH), the phase transformation of unstable FeOOH into soluble FeO_4^{2-} is prevented by V^{3+}, which guarantees the steady operation of the catalyst. In addition, the detachment of V^{5+} is much more favorable for creating a defective environment, thus benefiting the catalytic performance. These results again confirm that NiFeV-LDH is highly stable in alkaline medium. The extraordinary stability at high current density (75 h at 200 mA·cm^{-2}) of NiFeV-LDH is higher than that of the reported LDH-based materials (see Table S3), such as $Ni_{0.75}Fe_{0.125}V_{0.125}$-LDHs (15 h for 30 mA·$cm^{-2}$) [49], CoFeV-LDH (32 h for 30 mA·cm^{-2}) [38], Fe–Ni LDH (14 h for 10 mA·cm^{-2}) [19] and NiFe LDH/$NiCo_2O_4$ (10 h for 50 mA·cm^{-2}) [50].

As discussed above, compared to binary LDHs of NiFe-LDH or NiV-LDH, NiFeV-LDH possesses improved OER activity and long-term durability under high current density, which qualifies it as a promising OER electrocatalyst for commercialization. This can be attributed to three aspects. First, the crystallinity and electronic structure of the original binary LDH materials can be modified by the introduction of the third metal ion (V or Fe) to be a more favorable OER. In the ternary LDH, Fe mainly acts as the active site, while electron-withdrawing V can stabilize the high valence state of adjacent Fe, thus benefiting the OER. Second, V ions offer considerable stabilization for FeOOH generated in the surface reconstruction process, which is the real active species of OER, thus achieving superior long-term durability at high current densities. Third, Ni foam as the support and Ni source not only improves the conductivity of NiFeV-LDH but also considerably strengthens the mechanical strength through a closer interaction between active species and the substrate.

4 Conclusions

In summary, a self-supported NiFeV-LDH derived from Ni foam is developed via a simple and cost-saving hydrothermal method. Ni foam plays a dual role as a substrate and Ni source. Both transient and steady-state techniques were employed to determine the activity trend of the prepared catalysts. Under a moderate Fe:V ratio of 1:1, the optimized ternary NiFeV-LDHs display the best OER performance, requiring overpotentials of 269 and 274 mV at 50 mA·cm^{-2} (without *iR* compensation) in the LSV and SCV measurements, respectively. Compared to binary LDH materials, NiFeV-LDH exhibited an increased ECSA and improved charge transfer characteristics. The ECSA normalized current densities and TOF calculation results indicate that the approach of doping the third metal into the binary LDH materials can enhance the intrinsic OER performance. In addition, NiFeV-LDH exhibits excellent long-term durability (> 75 h) under extremely high current densities, such as 200 mA·cm^{-2}. Fe plays a crucial role as the active site in boosting the OER activity, while V contributes to the high stability of NiFeV-LDH. This work provides a new viewpoint for rationally designing active and highly stable electrocatalysts for the OER.

Acknowledgments This work is supported by the National Natural Science Foundation of China (Grant Nos. 22176017 and 21871028), CAS "Light of West China Program" (Grant No. XAB2020YW16), Scientific Research Project of the Ningxia Higher Education Department of China (Grant No. NGY2020034), Foundation of State Key Laboratory of High-efficiency Utilization of Coal and Green Chemical Engineering (Grant No. 2020-KF-40).

Electronic Supplementary Material Supplementary material is available in the online version of this article at https://dx.doi.org/10.1007/s11705-022-2179-6 and is accessible for authorized users.

References

1. da Silva Veras T, Mozer T S, da Costa Rubim Messeder dos Santos D, da Silva César A. Hydrogen: trends, production and characterization of the main process worldwide. International Journal of Hydrogen Energy, 2017, 42(4): 2018–2033
2. Kim J S, Kim B, Kim H, Kang K. Recent progress on multimetal oxide catalysts for the oxygen evolution reaction. Advanced Energy Materials, 2018, 8(11): 1702774
3. Suen N T, Hung S F, Quan Q, Zhang N, Xu Y J, Chen H M. Electrocatalysis for the oxygen evolution reaction: recent development and future perspectives. Chemical Society Reviews, 2017, 46(2): 337–365
4. Li Y, Sun Y, Qin Y, Zhang W, Wang L, Luo M, Yang H, Guo S. Recent advances on water-splitting electrocatalysis mediated by noble-metal-based nanostructured materials. Advanced Energy Materials, 2020, 10(11): 1903120
5. Wang Q, O'Hare D. Recent advances in the synthesis and application of layered double hydroxide (LDH) nanosheets. Chemical Reviews, 2012, 112(7): 4124–4155
6. Anantharaj S, Karthick K, Venkatesh M, Simha T V S V, Salunke

A S, Ma L, Liang H, Kundu S. Enhancing electrocatalytic total water splitting at few layer Pt−NiFe layered double hydroxide interfaces. Nano Energy, 2017, 39: 30–43

7. Hu L, Li M, Wei X, Wang H, Wu Y, Wen J, Gu W, Zhu C. Modulating interfacial electronic structure of CoNi LDH nanosheets with $Ti_3C_2T_x$ MXene for enhancing water oxidation catalysis. Chemical Engineering Journal, 2020, 398: 125605
8. Fan K, Chen H, Ji Y, Huang H, Claesson P M, Daniel Q, Philippe B, Rensmo H, Li F, Luo Y, Sun L. Nickel-vanadium monolayer double hydroxide for efficient electrochemical water oxidation. Nature Communications, 2016, 7(1): 11981
9. Goncalves J M, Martins P R, Angnes L, Araki K. Recent advances in ternary layered double hydroxide electrocatalysts for the oxygen evolution reaction. New Journal of Chemistry, 2020, 44(24): 9981–9997
10. Bi Y, Cai Z, Zhou D, Tian Y, Zhang Q, Zhang Q, Kuang Y, Li Y, Sun X, Duan X. Understanding the incorporating effect of Co^{2+}/Co^{3+} in NiFe-layered double hydroxide for electrocatalytic oxygen evolution reaction. Journal of Catalysis, 2018, 358: 100–107
11. Wang Z, Liu W, Hu Y, Xu L, Guan M, Qiu J, Huang Y, Bao J, Li H. An Fe-doped NiV LDH ultrathin nanosheet as a highly efficient electrocatalyst for efficient water oxidation. Inorganic Chemistry Frontiers, 2019, 6(7): 1890–1896
12. Anantharaj S, Kundu S, Noda S. "The Fe effect": a review unveiling the critical roles of Fe in enhancing OER activity of Ni and Co based catalysts. Nano Energy, 2021, 80: 105514
13. Anantharaj S, Karthick K, Kundu S. Evolution of layered double hydroxides (LDH) as high performance water oxidation electrocatalysts: a review with insights on structure, activity and mechanism. Materials Today. Energy, 2017, 6: 1–26
14. Nur Indah Sari F, Abdillah S, Ting J M. FeOOH-containing hydrated layered iron vanadate electrocatalyst for superior oxygen evolution reaction and efficient water splitting. Chemical Engineering Journal, 2021, 416: 129165
15. Bao W, Xiao L, Zhang J, Deng Z, Yang C, Ai T, Wei X. Interface engineering of NiV-LDH@FeOOH heterostructures as high-performance electrocatalysts for oxygen evolution reaction in alkaline conditions. Chemical Communications (Cambridge), 2020, 56(65): 9360–9693
16. Fan K, Ji Y, Zou H, Zhang J, Zhu B, Chen H, Daniel Q, Luo Y, Yu J, Sun L. Hollow iron-vanadium composite spheres: a highly efficient iron-based water oxidation electrocatalyst without the need for nickel or cobalt. Angewandte Chemie International Edition, 2017, 56(12): 3289–3293
17. Sun H, Xu X, Song Y, Zhou W, Shao Z. Designing high-valence metal sites for electrochemical water splitting. Advanced Functional Materials, 2021, 31(16): 2009779
18. Yu J, Yang F, Cheng G, Luo W. Construction of a hierarchical NiFe layered double hydroxide with a 3D mesoporous structure as an advanced electrocatalyst for water oxidation. Inorganic Chemistry Frontiers, 2018, 5(8): 1795–1799
19. Zeng L, Yang L, Lu J, Jia J, Yu J, Deng Y, Shao M, Zhou W. One-step synthesis of Fe−Ni hydroxide nanosheets derived from bimetallic foam for efficient electrocatalytic oxygen evolution and overall water splitting. Chinese Chemical Letters, 2018, 29(12): 1875–1878
20. Li P, Duan X, Kuang Y, Li Y, Zhang G, Liu W, Sun X. Tuning electronic structure of NiFe layered double hydroxides with vanadium doping toward high efficient electrocatalytic water oxidation. Advanced Energy Materials, 2018, 8(15): 1703341
21. Tang T, Jiang W J, Niu S, Liu N, Luo H, Chen Y Y, Jin S F, Gao F, Wan L J, Hu J S. Electronic and morphological dual modulation of cobalt carbonate hydroxides by Mn doping toward highly efficient and stable bifunctional electrocatalysts for overall water splitting. Journal of the American Chemical Society, 2017, 139(24): 8320–8328
22. Wang J X, Zhang Y, Capuano C B, Ayers K E. Ultralow charge-transfer resistance with ultralow Pt loading for hydrogen evolution and oxidation using Ru@Pt core-shell nanocatalysts. Scientific Reports, 2015, 5(1): 12220
23. Miyata S. Anion-exchange properties of hydrotalcite-like compounds. Clays and Clay Minerals, 1983, 31(4): 305–311
24. Forano C, Costantino U, Prévot V, Gueho C T. Developments in Clay Science. 2nd ed. Amsterdam: Elsevier, 2013: 745–782
25. Palapa N R, Saria Y, Taher T, Mohadi R, Lesbani A. Synthesis and characterization of Zn/Al, Zn/Fe, and Zn/Cr layered double hydroxides: effect of M^{3+} ions toward layer formation. Science and Technology Indonesia, 2019, 4(2): 36–39
26. Liu Y, Wang Y Z. Preparation and characterization of layered double hydroxide with different metallic ions. Chemical Research and Application, 2009, 21(6): 883–887
27. Schwertmann U, Pfab G. Structural vanadium in synthetic geothite. Geochimica et Cosmochimica Acta, 1994, 58(20): 4349–4352
28. Song Y, Song M, Liu P, Liu W, Yuan L, Hao X, Pei L, Xu B, Guo J, Sun Z. Fe-doping induced localized amorphization in ultrathin α-$Ni(OH)_2$ nanomesh for superior oxygen evolution reaction catalysis. Journal of Materials Chemistry A, 2021, 9(25): 14372–14380
29. Anantharaj S, Noda S. Amorphous catalysts and electrochemical water splitting: an untold story of harmony. Small, 2020, 16(2): 1905779
30. Nesbitt H W, Legrand D, Bancroft G M. Interpretation of Ni2p XPS spectra of Ni conductors and Ni insulators. Physics and Chemistry of Minerals, 2000, 27(5): 357–366
31. Feng Y, Li Z, Li S, Yang M, Ma R, Wang J. One stone two birds: vanadium doping as dual roles in self-reduced Pt clusters and accelerated water splitting. Journal of Energy Chemistry, 2022, 66: 493–501
32. Leng K, Zhang C, Li X, Hou C, Sun Y. Iron-containing MIL-101(Cr) as highly active and stable heterogeneous catalysts for the benzylation of aromatics with benzyl chloride. Reaction Kinetics, Mechanisms and Catalysis, 2017, 120(1): 345–357
33. Silversmit G, Depla D, Poelman H, Marin G B, De Gryse R. Determination of the V2p XPS binding energies for different vanadium oxidation states (V^{5+} to V^{0+}). Journal of Electron Spectroscopy and Related Phenomena, 2004, 135(2–3): 167–175
34. Wang J, Liao T, Wei Z, Sun J, Guo J, Sun Z. Heteroatom-doping of non-noble metal-based catalysts for electrocatalytic hydrogen evolution: an electronic structure tuning strategy. Small Methods, 2021, 5(4): 2000988

35. Yang Y, Dang L, Shearer M J, Sheng H, Li W, Chen J, Xiao P, Zhang Y, Hamers R J, Jin S. Highly active trimetallic NiFeCr layered double hydroxide electrocatalysts for oxygen evolution reaction. Advanced Energy Materials, 2018, 8(15): 1703189
36. Zhang B, Zheng X, Voznyy O, Comin R, Bajdich M, Garcia-Melchor M, Han L L, Xu J X, Liu M, Zheng L R, García de Arquer F P, Dinh C T, Fan F, Yuan M, Yassitepe E, Chen N, Regier T, Liu P, Li Y, De Luna P, Janmohamed A, Xin H L, Yang H, Vojvodic A, Sargent E H. Homogeneously dispersed multimetal oxygen-evolving catalysts. Science, 2016, 352(6283): 333–337
37. Bao J, Wang Z, Xie J, Xu L, Lei F, Guan M, Zhao Y, Huang Y, Li H. A ternary cobalt-molybdenum-vanadium layered double hydroxide nanosheet array as an efficient bifunctional electrocatalyst for overall water splitting. Chemical Communications (Cambridge), 2019, 55(24): 3521–3524
38. Hu Y, Wang Z, Liu W, Xu L, Guan M, Huang Y, Zhao Y, Bao J, Li H M. Novel cobalt-iron-vanadium layered double hydroxide nanosheet arrays for superior water oxidation performance. ACS Sustainable Chemistry & Engineering, 2019, 7(19): 16828–16834
39. Zhu Y X, Liu M, Hou G Y, Tang Y P, Wu L K. The release of metal ions induced surface reconstruction of layered double hydroxide electrocatalysts. Sustainable Energy & Fuels, 2021, 5(13): 3436–3444
40. Anantharaj S, Kundu S, Noda S. Worrisome exaggeration of activity of electrocatalysts destined for steady-state water electrolysis by polarization curves from transient techniques. Journal of the Electrochemical Society, 2022, 169(1): 014508
41. Anantharaj S, Ede S R, Karthick K, Sam Sankar S, Sangeetha K, Karthik P E, Kundu S. Precision and correctness in the evaluation of electrocatalytic water splitting: revisiting activity parameters with a critical assessment. Energy & Environmental Science, 2018, 11(4): 744–771
42. Zhang K, Zou R. Advanced transition metal-based OER electrocatalysts: current status, opportunities, and challenges. Small, 2021, 17(37): 2100129
43. Anantharaj S, Kundu S. Do the evaluation parameters reflect intrinsic activity of electrocatalysts in electrochemical water splitting? ACS Energy Letters, 2019, 4(6): 1260–1264
44. Anantharaj S, Karthik P E, Noda S. The significance of properly reporting turnover frequency in electrocatalysis research. Angewandte Chemie International Edition, 2021, 60(43): 23051–23067
45. Anantharaj S, Sugime H, Noda S. Surface amorphized nickel hydroxy sulphide for efficient hydrogen evolution reaction in alkaline medium. Chemical Engineering Journal, 2021, 408: 127275
46. Trotochaud L, Young S L, Ranney J K, Boettcher S W. Nickel-iron oxyhydroxide oxygen-evolution electrocatalysts: the role of intentional and incidental iron incorporation. Journal of the American Chemical Society, 2014, 136(18): 6744–6753
47. Sun M, Ru X R, Zhai L F. In-situ fabrication of supported iron oxides from synthetic acid mine drainage: high catalytic activities and good stabilities towards electro-Fenton reaction. Applied Catalysis B: Environmental, 2015, 165: 103–110
48. Bai J, Mei J, Liao T, Sun Q, Chen Z G, Sun Z. Molybdenum-promoted surface reconstruction in polymorphic cobalt for initiating rapid oxygen evolution. Advanced Energy Materials, 2022, 12(5): 2103247
49. Dinh K N, Zheng P L, Dai Z F, Zhang Y, Dangol R, Zheng Y, Li B, Zong Y, Yan Q Y. Ultrathin porous NiFeV ternary layer hydroxide nanosheets as a highly efficient bifunctional electrocatalyst for overall water splitting. Small, 2018, 14(8): 1703257
50. Wang Z, Zeng S, Liu W, Wang X, Li Q, Zhao Z, Geng F. Coupling molecularly ultrathin sheets of NiFe-layered double hydroxide on $NiCo_2O_4$ nanowire arrays for highly efficient overall water-splitting activity. ACS Applied Materials & Interfaces, 2017, 9(2): 1488–1495